machines

MDPI

Article

Finite Speed-Set Model Reference Adaptive System Based on Sensorless Control of Permanent Magnet Synchronous Generators for Wind Turbines

Mohammed A. Hassan [1,2,*], Mahmoud M. Adel [1], Ahmed Farhan [1] and Amr A. Saleh [1]

[1] Electrical Engineering Department, Faculty of Engineering, Fayoum University, Fayoum 63514, Egypt; mma24@fayoum.edu.eg (M.M.A.); afm01@fayoum.edu.eg (A.F.); aae00@fayoum.edu.eg (A.A.S.)
[2] Electrical Engineering Department, College of Engineering, King Faisal University, Al Ahsa 31982, Saudi Arabia
* Correspondence: m.hassan@kfu.edu.sa or mah03@fayoum.edu.eg; Tel.: +966-135895429

Abstract: This paper proposes a novel finite speed-set model reference adaptive system (FSS-MRAS) based on the current predictive control (CPC) of a permanent magnet synchronous generator (PMSG) in wind energy turbine systems (WETSs). The mathematical models of wind energy systems (WESs) coupled with a permanent magnet synchronous generator (PMSG) are presented in addition to the implementation of the CPC of PMSGs. The proposed FSS-MRAS is based on eliminating the tuning burden of the conventional MRAS by using a limited set of speeds of the PMSG rotor that are employed to predict the rotor speed of the generator. Consequently, the optimal speed of the rotor is the one resulting from the optimization of a proposed new cost function. Accordingly, the conventional MRAS controller is eliminated and the main disadvantage represented in the tuning burden of the constant-gain proportional-integral (PI) controller has been overcome. The proposed FSS-MRAS observer is validated using MATLAB/Simulink (R2023b) at different operating conditions. The results of the proposed FSS-MRAS have been compared with those of the conventional MRAS, which proved the high robustness and reliability of the proposed observer.

Keywords: permanent magnet synchronous generator; model predictive control; model reference adaptive system; sensor-less control; wind turbines

Citation: Hassan, M.A.; Adel, M.M.; Farhan, A.; Saleh, A.A. Finite Speed-Set Model Reference Adaptive System Based on Sensorless Control of Permanent Magnet Synchronous Generators for Wind Turbines. *Machines* **2024**, *12*, 429. https://doi.org/10.3390/machines12070429

Received: 25 May 2024
Revised: 15 June 2024
Accepted: 17 June 2024
Published: 24 June 2024

1. Introduction

The production of electricity from renewable energy sources such as wind turbines has grown dramatically in recent years, which has reduced environmental pollution and carbon dioxide emissions [1]. It has been demonstrated that wind power is a viable method of electricity generation with little influence on the environment [2].

In today's wind turbine applications, two generators are well-known: the permanent magnet synchronous generator (PMSG) and the doubly fed induction generator (DFIG) [3]. Due to their many advantages over fixed speed induction generators or synchronous generators with full-sized converters, variable speed, decoupled active and reactive power control capabilities, lower converter cost, and lower power losses, doubly fed induction generators (DFIG) have become more and more popular for wind power generation. However, the main disadvantages of DFIGs are their high sensitivity to grid faults, the existence of a gear box which causes noise, their big size, and their requiring frequent maintenance [4].

Such drawbacks of the DFIG encourage the utilization of the direct-driven PMSG, which in addition has many other advantages represented in its high efficiency, great power density, lower size, full controllability, and its low sensitivity to grid faults due to its isolation via back-to-back converters [4,5].

Many control algorithms have been developed by researchers to obtain the maximum wind turbine output power [6,7]. Vector control approaches—such as field-oriented control

(FOC), which employs PI controllers—are commonly used for the purpose of controlling the PMSG to harvest the optimum power of the wind turbine [8]. The main disadvantages of the FOC approach are the existence of PI controllers (which requires the tuning of proportional and integral parameters), slow response dynamics, and the need for modulation [5]. Hence, many advanced control approaches have been developed by researchers to overcome these drawbacks, such as model predictive control (MPC). Thanks to the rapid development of microprocessors, researchers have in turn been encouraged to consider the MPC in control of the PMSG to track the wind turbine's optimum power [9].

There are two variants of MPC: continuous-set model predictive control (CS-MPC), which needs a modulation phase to produce switching actions, and finite-set model predictive control (FS-MPC), which takes into account a finite number of switching actions [10]. The primary characteristic of predictive control is the employment of a system model to forecast the predicted behavior of the controlled variables. The controller uses these data to calculate the optimal actuation based on a predefined optimization criterion, which is represented as a cost function that has to be minimized [1]. In this paper, finite-set model predictive control is employed to accomplish the optimum power of the wind turbine.

The PMSG's position and speed may be determined using speed sensors, such as Hall effect sensors, resolvers, or encoders. Nonetheless, researchers are encouraged to exclude speed sensors due to their disadvantages, including their exorbitant cost and the need for frequent maintenance. The primary substitute method employs sensor-less control techniques to estimate position and speed [11]. For PMSGs, researchers have presented a number of sensor-less control methods. These methods can be divided into two main categories. The model reference adaptive system, extended Kalman filter (EKF), and sliding mode observer (SMO) are examples of machine models that form the basis of the first category. The second category, which is favored for low speeds, is based on anisotropic techniques such as high-frequency injection methods [11]. The EKF method's primary weakness is its featuring complicated computations caused by several matrix multiplications. The discontinuous switching control of the SMO approach, which affects the control accuracy, is its primary drawback [12]. Due to its key advantages, such as its low computing effort, ease of implementation, strong stability, and accurate position estimation, the MRAS is one of the most widely used sensor-less algorithms for speed estimation [13]. However, one of the main drawbacks of the MRAS approach is the existence of the PI controller, which requires accurate tuning of the proportional and integral terms to obtain the best speed/position estimation performance. In addition, these tuning factors are not suitable for the whole speed range, which led researchers to present adaptive techniques to overcome the tuning drawback. Hence, the proposed technique presents a novel finite -set speed MRAS which eliminates the conventional MRAS controller and consequently overcomes the tuning burden of the MRAS PI controller.

In [14], the generator-side converter is controlled by field-oriented control with voltage space vector PWM. The field-oriented control method allows for the optimization of tip speed ratio and optimum wind energy capture while achieving the best possible efficiency for wind generators. In Ref. [15], a fuzzy logic controller is implemented to control the outer speed loop, while a new anti-windup PI controller is used to build the inner current loop. Additionally, Ref. [16] provided a model for a wind turbine that concurrently takes into account mechanical, electrical, and aerodynamic factors in addition to the employment of a yaw mechanism to reduce and regulate the wind turbine's excessive output power at high wind speeds without the need for additional hardware. In [17], a permanent magnet synchronous generator-based variable-speed wind energy conversion system's robust power generation control technique was proposed, which combined a field-oriented sliding mode-based control method with a reliable observer of the aerodynamic torque. In Ref. [18], sensor-less control methods for an offshore wind farm that utilized the extended Kalman filter to determine the estimated rotor position/speed for a PMSG are suggested. Furthermore, Ref. [6] developed an algorithm that reduced the PMSG's loss and conducted the operation at optimal power, in addition to employing the model reference

adaptive system (MRAS) to estimate the PMSG's position/speed. In Ref. [19], a novel phase locked loop (PLL) with a finite position-set for the sensorless FOC of a PMSG is suggested. In [20,21], different algorithms have been presented to be more suitable for digital signal processing (DSP) by reducing the number of iterations for a finite position-set PLL for the PMSG. Further, Ref. [22] proposed an MRAS algorithm which excluded the PI controller, with a finite position-set based on a certain number of rotor positions for micro-grid systems' PMSGs.

This paper presents the model predictive control of the permanent magnet synchronous generator for direct-driven wind turbine systems. In order to find the optimal tracking of the wind turbine's output power, the PMSG's accurate speed is needed. Hence, a novel finite speed-set MRAS (FSS-MRAS) algorithm is employed to estimate the PMSG's speed/position. The main contribution in the proposed technique is excluding the PI controller of the conventional MRAS's adaptive mechanism by the employment of the finite speed-set algorithm in which certain rotor speeds are defined and a predicted cost function is calculated for each predicted estimated speed. The cost function of the proposed finite speed-set MRAS is defined as the input error of the conventional MRAS PI controller which shall converge to zero. The authors in [20,22] have developed a finite position-set MRAS based on a certain number of rotor positions for the PMSGs. A limited-position-set MRAS estimator replaced the incremental encoder for the control of DFIGs in wind turbine systems in [23]. The novelty in the presented method is that the finite speed-set MRAS is proposed based on a certain number of rotor speeds with a relatively low number of iterations, which makes the proposed algorithm more suitable for the digital signal processing (DSP). Also, the accuracy of the estimation of the proposed approach is validated by the comparison between the proposed finite speed-set MRAS estimated speed, conventional MRAS estimated speed, and measured actual speed. One of the main points of strength for the proposed approach is the absence of a tuning burden for both the PMSG MPC and the proposed FSS-MRAS estimation technique.

The rest of the paper is organized as follows. The system model including the mathematical modeling of the wind turbine, the modeling of the PMSG, and the two-level three-phase inverter are indicated in Section 2. Section 3 presents the current predictive control finite-set of a PMSG. In Section 4, the proposed finite speed-set MRAS (FSS-MRAS) and the traditional one are presented. The simulation results, including a performance comparison between the conventional MRAS and the proposed FSS-MRAS for PMSG, are illustrated and discussed in Section 5. Section 6 presents the paper's conclusion.

2. System Model

2.1. Wind Turbine Modeling

The main components of a variable-speed wind energy conversion system are converters, a generator, and a wind turbine. In fact, the rotor blades collect the kinetic energy of the wind and convert it to mechanical energy, which the generator then converts to electrical energy.

The modeling equations of the wind turbine systems are given in [24,25]. The wind power generated from the wind turbine can be calculated as follows:

$$P_w = \frac{1}{2}mv_w^2 = \frac{1}{2}\rho V_t v_w^2 = \frac{1}{2}\rho A_t v_w^3 = \frac{1}{2}\rho\pi r_t^2 v_w^3 \quad (1)$$

where P_w is the wind power, m is the air mass, v_w is the wind speed, V_t is the air volume, A_t is the cross-sectional area traversed by the wind, r_t is the radius and ρ is the air density.

The tip speed ratio can be calculated as follows:

$$\lambda = \frac{\omega_m r_t}{v_w} \quad (2)$$

where ω_m is the mechanical speed of the generator. The power coefficient by which the wind energy is converted to output mechanical energy can be determined as follows:

$$C_p = 0.5176\left(\frac{116}{\lambda_i} - 0.4\beta - 5\right)^{\frac{-21}{\lambda_i}} + 0.0068\lambda \tag{3}$$

$$\lambda_i = \frac{1}{\frac{1}{\lambda + 0.08\beta} - \frac{0.035}{\beta^3 + 1}} \tag{4}$$

where β is the pitch angle. The output mechanical power and torque of the wind turbine can be determined from the following equations:

$$P_t = C_p P_w = \frac{1}{2} C_p \rho \pi r_t^2 v_w^3 \tag{5}$$

$$T_t = \frac{P_t}{\omega_m} \tag{6}$$

Figure 1 shows the power coefficient curves (C_p) vs. the tip speed ratio (λ) at a zero blade pitch angle (β) value [26].

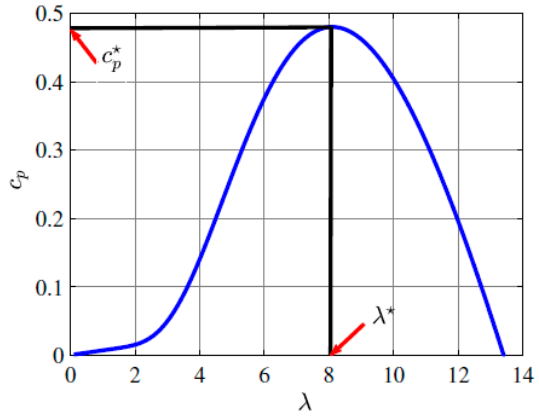

Figure 1. C_p vs. λ at $\beta = 0$ [26].

2.2. Modeling of Permanent Magnet Synchronous Generator

The following is the derivation of the PMSG's mathematical modeling equations in the dq0 rotating reference frame [22,27]:

$$\boldsymbol{\lambda}_{dq} = L_{dq}\mathbf{I}^r_{dq} + \boldsymbol{\psi}_s \tag{7}$$

$$\mathbf{V}^r_{dq} = \mathbf{R}_s\mathbf{I}^r_{dq} + \frac{d}{dt}\boldsymbol{\lambda}_{dq} + \omega_r\, J\, \boldsymbol{\lambda}_{dq} \tag{8}$$

$$T_e = \frac{3}{2}\frac{P}{2}\left[\lambda_m i^r_q + (L_d - L_q) i^r_q i^r_d\right] \tag{9}$$

$$\frac{d\omega_m}{dt} = \frac{1}{j}(T_e - T_m - B\omega_m) \tag{10}$$

where $\boldsymbol{\lambda}_{dq} = \begin{pmatrix}\lambda_d\\ \lambda_d\end{pmatrix}$, $\mathbf{L}_{dq} = \begin{bmatrix}L_d & 0\\ 0 & L_q\end{bmatrix}$, $\boldsymbol{\psi}_s = \begin{pmatrix}\lambda_m\\ 0\end{pmatrix}$, $\mathbf{V}^r_{dq} = \begin{pmatrix}v^r_d\\ v^r_q\end{pmatrix}$, $\mathbf{I}^r_{dq} = \begin{pmatrix}i^r_d\\ i^r_q\end{pmatrix}$, $\mathbf{R}_s = \begin{bmatrix}r_s & 0\\ 0 & r_s\end{bmatrix}$, $\mathbf{J} = \begin{bmatrix}0 & -1\\ 1 & 0\end{bmatrix}$.

Here $\boldsymbol{\lambda}_{dq}$, $\mathbf{I}^r_{dq}$, $\mathbf{V}^r_{dq}$ are fluxes, currents, and stator voltages in the rotating reference frame. (ω_m,ω_r) are the mechanical and electrical speeds of the PMSG rotor, r_s is the winding resistance of the PMSG stator. λ_m is the magnetic flux linkage of the PMSG rotor,

T_e is the electromagnetic torque, T_m is the PMSG mechanical torque, B is the PMSG viscous friction, P is the number of poles, and j is the PMSG inertia.

As the wind turbine is coupled to the PMSG, the PMSG mechanical torque is equal to the output mechanical power of the wind turbine calculated in Equation (6) and the PMSG mechanical torque can be given as follows:

$$T_m = -T_t \tag{11}$$

2.3. Inverter Model

The two-level three-phase inverter is the most common inverter used in power drive applications. Hence, it is used to produce the three-phase voltage of the PMSG as shown in Figure 2 [28]. This sort of inverter can generate eight voltage vectors from eight switching states, as illustrated in [29]. The inverter coupled to the PMSG to supply three-phase voltages is shown in Figure 2. Equation (12), which is written in terms of the switching vector of the inverter, computes the output voltages of the PMSM in the *dq* synchronous rotating reference frame after applying Clarke and Park transformations [30].

$$v_{dq}^{r} = \begin{bmatrix} \cos\theta_r & \sin\theta_r \\ -\sin\theta_r & \cos\theta_r \end{bmatrix} \frac{2}{3} \begin{bmatrix} 1 & -\frac{1}{2} & -\frac{1}{2} \\ 0 & \frac{\sqrt{3}}{2} & -\frac{\sqrt{3}}{2} \end{bmatrix} \frac{1}{3} V_{dc} \begin{bmatrix} 2 & -1 & -1 \\ -1 & 2 & -1 \\ -1 & -1 & 2 \end{bmatrix} S_s^{abc} \tag{12}$$

where θ_r, S_s^{abc}, V_{dc} is the electrical rotor position, switching vector and dc-link voltage, respectively.

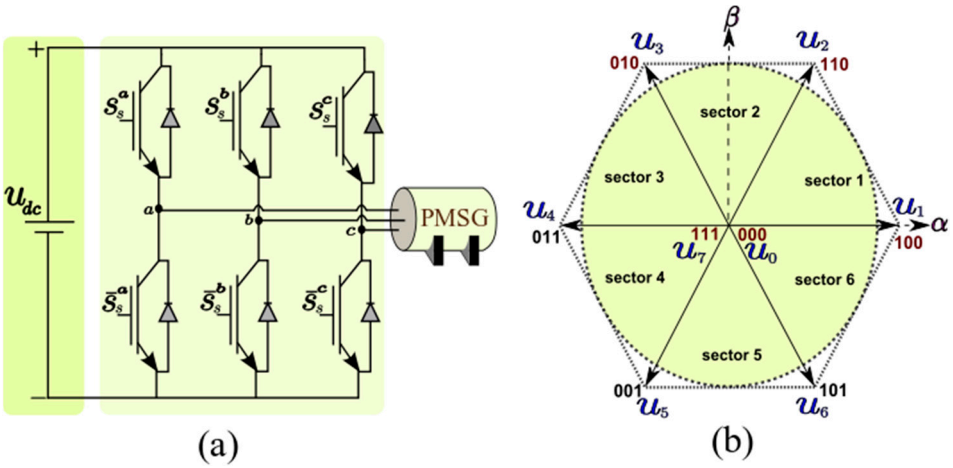

Figure 2. Two-level three-phase inverter: (**a**) PMSG fed by a three-phase inverter, and (**b**) voltage space vectors [31,32].

3. Current Predictive Control Finite Set of PMSG

The turbine generates its maximum power at a certain maximum power coefficient C_p^*. Consequently, this number is thought to be optimal for the turbine's highest performance. However, the best tip speed ratio (λ^*) determines this. From Figure 1, the ideal tip speed ratio (λ^*) is 8.11 and (C_p^*) is around 0.48 for $\beta = 0$.

The primary goal of PMSG control is to ensure that maximum power point tracking (MPPT) criteria are met in PMSG-based variable-speed wind turbines by regulating the electromagnetic torque of the PMSG [22]. Hence, the reference electromagnetic torque of the PMSG is achieved by capturing the optimal output wind turbine mechanical power (P_t^*) [26]. The maximum output mechanical power of the wind turbine (P_t^*) can be obtained by achieving the optimal power coefficient (C_p^*).

$$P_t^* = \frac{1}{2} C_p^* \rho \pi r_t^2 v_w^3 \tag{13}$$

Based on Equation (2), the optimal mechanical power and torque of the wind turbine can be given as follows:

$$P_t^* = \frac{1}{2} C_p^* \rho \pi r_t^2 \left(\frac{r_t \omega_m}{v_w}\right)^3 = \frac{1}{2} C_p^* \rho \pi r_t^5 \left(\frac{\omega_m}{\lambda^*}\right)^3 \tag{14}$$

$$T_t^* = \frac{P_t^*}{\omega_m} = \frac{1}{2} \rho \pi r_t^5 \frac{C_p^*}{(\lambda^*)^3} \omega_m^2 \tag{15}$$

From Equation (2), the optimal mechanical speed (ω_m^*) can be calculated by achieving the best tip speed ratio as follows:

$$\omega_m^* = \frac{v_w \lambda^*}{r_t} \tag{16}$$

Using Equation (15), the reference PMSG electromagnetic torque (T_m^*) can be defined by the optimal mechanical torque of the wind turbine as follows:

$$T_m^* = -T_t^* = -\frac{1}{2} \rho \pi r_t^5 \frac{C_p^*}{(\lambda^*)^3} \omega_m^2 \tag{17}$$

To perform model predictive control and obtain the following predicted sampling instant states, the PMSM continuous time model has to be discretized. Therefore, it is possible to predict the PMSM currents' future instants as follows:

$$i_d(k+1) = \left(1 - \frac{R_s T_s}{L_d}\right) i_d(k) + T_s \omega_r(k) i_q(k) + \frac{T_s}{L_d} v_d(k) \tag{18}$$

$$i_q(k+1) = \left(1 - \frac{R_s T_s}{L_q}\right) i_q(k) - T_s \omega_r(k) i_d(k) + \frac{T_s}{L_q} v_q(k) - \frac{T_s \lambda_m}{L_q} \omega_r(k) \tag{19}$$

where $i_d(k+1)$ and $i_q(k+1)$ are the next state's stator currents which are determined by taking the current stator currents, voltages, and speed $i_q(k), i_d(k), v_q(k), v_d(k)$ and $\omega_r(k)$. T_s is the sample time.

Equation (12) can be employed to derive the stator voltages v_{dq}. Using Equations (18) and (19), the seven inverter voltage vectors are used to obtain the seven predicted values of the stator currents. A cost function is then used to determine which inverter vector is best to apply to the PMSG [33].

The d-axis reference is set to zero to achieve the maximum torque per ampere ($i_{dref} = 0$) and the q-axis reference current of the PMSG can be calculated for the reference PMSG electromagnetic torque from the below equations:

$$i_{q\ ref}(k+1) = \frac{T_m^*}{K_t} = \frac{-T_t^*}{K_t} \tag{20}$$

$$K_t = \frac{3}{2} \frac{P}{2} \lambda_m \tag{21}$$

The cost function is calculated as the sum of the error absolute values between the predicted currents $[i_d(k+1), i_q(k+1)]$ and the reference currents $[i_{d\ ref}, i_{q\ ref}]$, respectively. The cost function is defined in Equation (22).

$$g = |i_{d\ ref} - i_d(k+1)| + \left|i_{q\ ref} - i_q(k+1)\right| \tag{22}$$

The best inverter switching vector is chosen such that the lowest cost function is attained.

4. Proposed and Traditional Observers

4.1. Traditional MRAS for PMSGs

Since the MRAS is so easy to implement, it is frequently used to estimate a PMSG's speed and position. The MRAS uses two models: an adaptive model and a reference model. In Figure 3, the traditional MRAS approach is displayed [34,35].

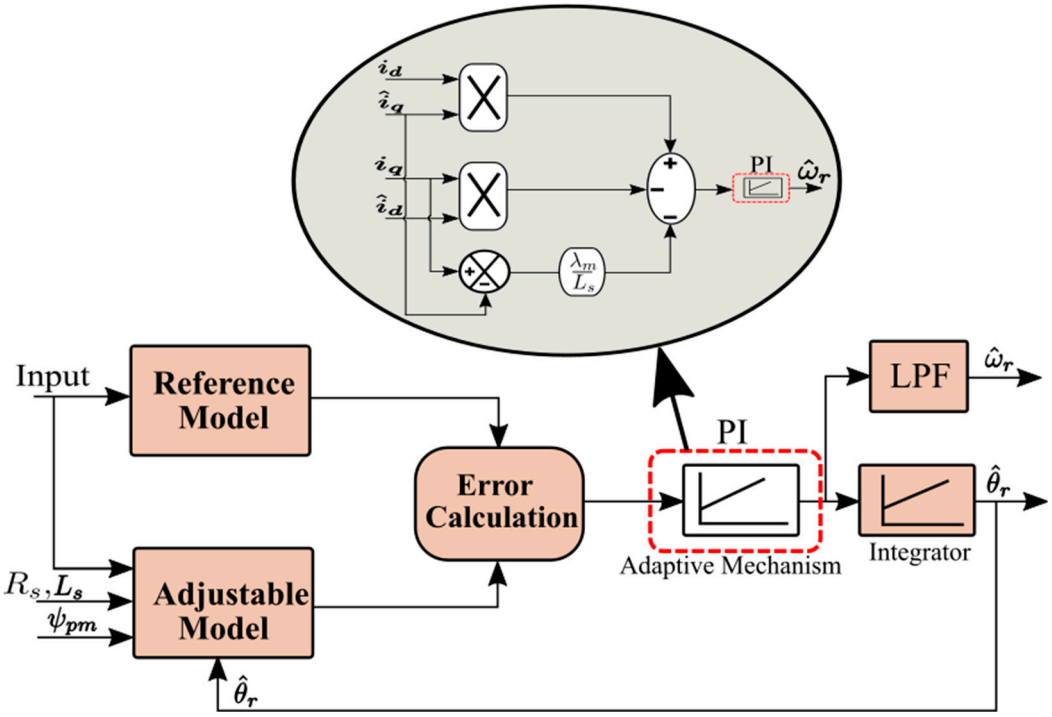

Figure 3. Traditional MRAS estimator block diagram.

The motor variable used by the MRAS is a state variable that is derived from both the adjustable and reference models. The stator current calculated from the reference model and the stator current determined by the adjustable model are used in an adaptation model and an adaption mechanism [34]. Figure 3 shows the adaptive mechanism block diagram of the conventional MRAS. The equations of the traditional MRAS algorithm are described as follows:

$$\frac{di_d}{dt} = -\frac{r_s}{L_d} i_d + \omega_r \frac{L_q}{L_d} i_q + \frac{v_d}{L_d} \tag{23}$$

$$\frac{di_q}{dt} = -\frac{r_s}{L_q} i_q - \omega_r \frac{L_d}{L_q} i_d + \frac{v_q}{L_q} - \omega_r \frac{\lambda_m}{L_q} \tag{24}$$

i_d^*, i_q^*, v_d^*, v_q^* are defined as follows:

$$i_d^* = i_d + \frac{\lambda_m}{L_d}, i_q^* = i_q \tag{25}$$

$$v_d^* = v_d + \frac{r_s}{L_d}\lambda_m, v_q^* = v_q \tag{26}$$

From Equations (25) and (26),

$$\frac{di_d^*}{dt} = -\frac{r_s}{L_d} i_d^* + \hat{\omega}_r \frac{L_q}{L_d} i_q^* + \frac{v_d^*}{L_d} \tag{27}$$

$$\frac{di_q^*}{dt} = -\frac{r_s}{L_q} i_q^* - \hat{\omega}_r \frac{L_d}{L_q} i_d^* + \frac{v_q^*}{L_q} - \hat{\omega}_r \frac{\lambda_m}{L_q} \tag{28}$$

The estimated speed can be determined in

$$\hat{\omega}_r = \left(K_p + \frac{K_i}{s}\right)\left[\frac{L_q}{L_d} i_d \hat{i}_q - \frac{L_d}{L_q}\hat{i}_d i_q - \frac{\lambda_m}{L_q}(i_q - \hat{i}_q) + \hat{i}_q \hat{i}_d \left(\frac{L_d}{L_q} - \frac{L_q}{L_d}\right)\right] \quad (29)$$

It is clear from Figure 3 that the adaptive mechanism of the classical MRAS requires a PI controller, which leads to one of the main drawbacks, represented in the need to accurate tuning to obtain a precise speed/position estimation. This disadvantage unfortunately represents a burden which is overcome in the proposed method by excluding the PI controller of the adaptation mechanism.

4.2. Proposed Finite Speed-Set MRAS (FSS-MRAS) of PMSGs

As discussed in Section 4.1, it is obvious that one of the primary drawbacks of the classical MRAS is the existence of the PI controller in the MRAS adaptation mechanism. Hence, the proposed finite speed-set MRAS (FSS-MRAS) approach omits the PI controller of the adaptation mechanism to overcome the tuning difficulty. The suggested FSS-MRAS uses reference and adjustable models that are equivalent to those of the conventional one. The proposed FSS-MRAS concept is based on the FCS-MPC. In the proposed FSS-MRAS, a certain number of electrical angular rotor speeds, similar to the eight switching vectors in the FCS-MPC, are defined. Using this particular number of speeds, the actual measured currents in the *abc* frame which represent the reference model are transformed to the *dq* frame; in addition, the currents are calculated using the adjustable model. In the proposed FSS-MRAS, the error of the traditional MRAS PI controller represents the predefined cost function which shall be minimized by one of the defined number of speeds. So, the error between the reference model and the adjustable model is predicted for each speed defined by the FSS-MRAS. Finally, the estimated predicted speed is the one that leads to the minimization of the investigated cost function. Hence, the main difference between the traditional MRAS and the proposed FSS-MRAS is that the error between the reference model and the adjustable model are minimized by the employment of the PI controller in the conventional MRAS, while the error in the proposed FSS-MRAS is minimized by the employment of a cost function which is calculated for each defined speed of the FSS-MRAS, and the speed with the lowest cost function is selected to be the estimated speed for this sampling time. The block diagram for the proposed FSS-MRAS is shown in Figure 4.

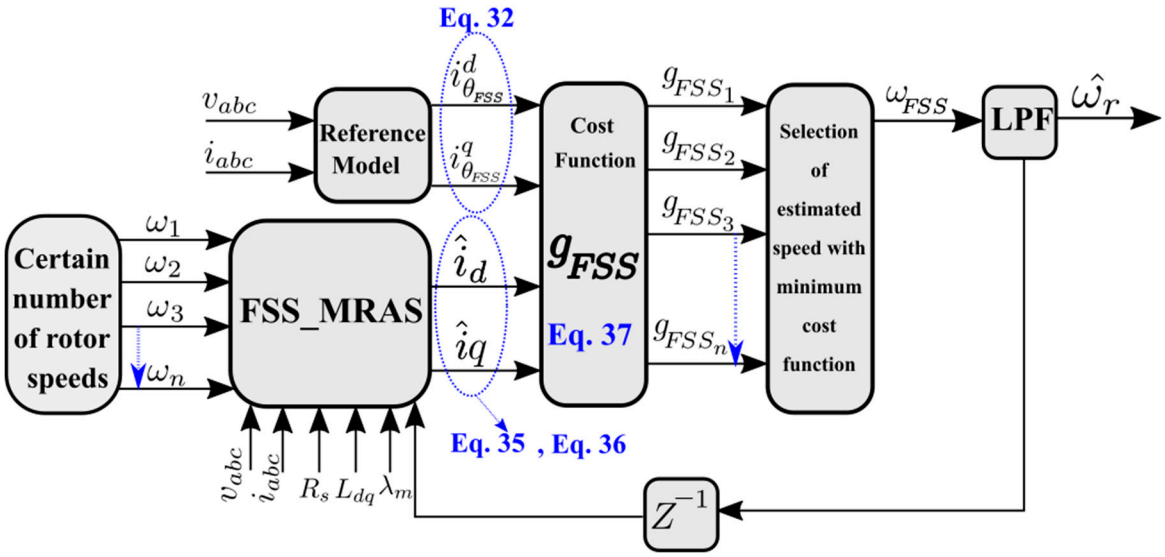

Figure 4. Block diagram for the proposed FSS-MRAS observer.

The equations of the proposed FSS-MRAS are shown below. Firstly, a certain number of electrical angular rotor speeds are defined in a similar way to the switching vectors

of the FCS-MPC and a predicted estimated position is calculated for each defined speed as follows:

$$\theta_{FSS}(k+1) = \omega_{FSS} * T_s + \theta_{FSS}(k) \tag{30}$$

where ω_{FSS} is the number of defined speeds of the proposed FSS-MRAS, θ_{FSS} is the predicted position of the FSS-MRAS and T_s is the sampling time.

Secondly, the actual measured currents in the abc frame are transformed to the αβ stationary frame according to Equation (31). Then, the measured currents in the αβ stationary frame are transformed to the rotating synchronous dq frame using the estimated predicted position (θ_{FSS}) for each defined speed in Equation (32).

$$i_{\alpha\beta} = \frac{2}{3}\begin{bmatrix} 1 & -\frac{1}{2} & -\frac{1}{2} \\ 0 & \frac{\sqrt{3}}{2} & -\frac{\sqrt{3}}{2} \end{bmatrix}\begin{bmatrix} i_a \\ i_b \\ i_c \end{bmatrix} \tag{31}$$

$$\begin{bmatrix} i_d \\ i_q \end{bmatrix} = \begin{bmatrix} \cos\theta_{FSS} & \sin\theta_{FSS} \\ -\sin\theta_{FSS} & \cos\theta_{FSS} \end{bmatrix}\begin{bmatrix} i_\alpha \\ i_\beta \end{bmatrix} \tag{32}$$

The currents calculated (i_d, i_q) in Equation (32) represent the reference model of the proposed FSS-MRAS. After the calculation of the reference model currents, the adjustable model currents shall be calculated. The measured voltages in the abc frame are transformed to the αβ stationary frame according to Equation (33). Then, the measured voltages in the αβ stationary frame are transformed to the rotating synchronous dq frame using the estimated predicted position (θ_{FSS}) for each defined speed in Equation (34).

$$v_{\alpha\beta} = \frac{2}{3}\begin{bmatrix} 1 & -\frac{1}{2} & -\frac{1}{2} \\ 0 & \frac{\sqrt{3}}{2} & -\frac{\sqrt{3}}{2} \end{bmatrix}\begin{bmatrix} v_a \\ v_b \\ v_c \end{bmatrix} \tag{33}$$

$$\begin{bmatrix} \hat{v}_d \\ \hat{v}_q \end{bmatrix} = \begin{bmatrix} \cos\theta_{FSS} & \sin\theta_{FSS} \\ -\sin\theta_{FSS} & \cos\theta_{FSS} \end{bmatrix}\begin{bmatrix} v_\alpha \\ v_\beta \end{bmatrix} \tag{34}$$

The voltages calculated ($\hat{v}_d$, $\hat{v}_q$) in Equation (34) represent the adjustable model estimated voltages of the proposed FSS-MRAS for each defined speed. The currents of the adjustable model are calculated based on the discrete time model of the PMSG and by the employment of the estimated predicted voltage and the estimated predicted position for each defined speed as follows:

$$\hat{i}_d = \left(1 - \frac{R_s T_s}{L_d}\right)\hat{i}_d(k) + T_s\,\omega_{FSS}\,\hat{i}_q(k) + \frac{T_s}{L_d}\hat{v}_d(k) \tag{35}$$

$$\hat{i}_q = \left(1 - \frac{R_s T_s}{L_q}\right)\hat{i}_q(k) - T_s\,\omega_{FSS}\,\hat{i}_d(k) + \frac{T_s}{L_q}\hat{v}_q(k) - \frac{T_s\lambda_m}{L_q}\omega_{FSS} \tag{36}$$

The currents calculated ($\hat{i}_d$, $\hat{i}_q$) in Equations (35) and (36) represent the adjustable model's estimated predicted currents of the proposed FSS-MRAS for each defined speed. The cost function of the proposed FSS-MRAS is the error calculation for the traditional MRAS PI controller which is calculated using the currents of the reference model and adjustable model and can be described as follows:

$$g_{FSS} = \left|\frac{L_q}{L_d} i_d \hat{i}_q - \frac{L_d}{L_q}\hat{i}_d i_q - \frac{\lambda_m}{L_q}\left(i_q - \hat{i}_q\right) + \hat{i}_q\hat{i}_d\left(\frac{L_d}{L_q} - \frac{L_q}{L_d}\right)\right| \tag{37}$$

where i_d, i_q are the reference model states of the measured currents transformed from the abc frame to the dq frame using the defined speeds of the FSS-MRAS from Equation (32), and $\hat{i}_d$ and $\hat{i}_q$ are the adjustable model states of the currents calculated using the defined speeds of the FSS-MRAS from Equations (35) and (36).

The proposed FSS-MRAS algorithm can be presented as follow Algorithm 1:

Algorithm 1. Algorithm of the proposed FSS-MRAS

Step 1
Read v_a, $v_b v_c$, i_a, i_b, i_c

Step 2
Transform v_a, v_b, v_c, i_a, i_b, i_c to $v_{\alpha\beta}$ and $i_{\alpha\beta}$ using Equations (31) and (33)

Step 3
Define the speed change direction (increasing or decreasing)
$\omega_1 = \omega(k) + \Delta\omega$
$\omega_2 = \omega(k) - \Delta\omega$
Calculate the predicted position from Equation (30)
Calculate i_d, i_q from Equation (32) for both ω_1 and ω_2
Calculate $\hat{v}_d$, $\hat{v}_q$ from Equation (34) for both ω_1 and ω_2
Calculate $\hat{i}_d$, $\hat{i}_q$ from Equations (35) and (36) for both ω_1 and ω_2
Calculate the cost functions g_1 and g_2 from Equation (37) for both ω_1 and ω_2 respectively.
Note: if $g_1 < g_2$ then the right direction is increasing, else the right direction is decreasing.

Step 4
If $g_1 < g_2$ then
Define the finite speed-set starting from the old speed in positive direction.
For $\omega_{FSS} = \omega_{Fss}(k) : 1 : \omega_{nom}$ (ω_{nom} is the rated electrical angular speed)
Calculate the predicted position from Equation (30)
Calculate i_d, i_q from Equation (32) for ω_{FSS}
Calculate $\hat{v}_d$, $\hat{v}_q$ from Equation (34) for ω_{FSS}
Calculate $\hat{i}_d$, $\hat{i}_q$ from Equations (35) and (36) for $\omega_{FSS\ MRAS}$
$g_{FSS} = \text{abs}\left[\frac{L_q}{L_d} i_d \hat{i}_q - \frac{L_d}{L_q} \hat{i}_d i_q - \frac{\lambda_m}{L_q}(i_q - \hat{i}_q) + \hat{i}_q \hat{i}_d \left(\frac{L_d}{L_q} - \frac{L_q}{L_d}\right)\right]$
If $g_{FSS} < g_{opt}$
$g_{opt} = g_{FSS}$
$\omega_{opt} = \omega_{FSS}$
End
If g_{opt} < accepted tolerance
Break
End
End
$\hat{\omega}_r = \omega_{opt}$

elseif $g_1 > g_2$ then
Define the finite speed-set starting from the old speed in negative direction
For $\omega_{FSS} = \omega_{Fss}(k) : -1 : 0$
Calculate the predicted position from Equation (30)
Calculate i_d, i_q from Equation (32) for ω_{FSS}
Calculate $\hat{v}_d$, $\hat{v}_q$ from Equation (34) for ω_{FSS}
Calculate $\hat{i}_d$, $\hat{i}_q$ from Equations (35) and (36) for $\omega_{FSS\ MRAS}$
$g_{FSS} = \text{abs}\left[\frac{L_q}{L_d} i_d \hat{i}_q - \frac{L_d}{L_q} \hat{i}_d i_q - \frac{\lambda_m}{L_q}(i_q - \hat{i}_q) + \hat{i}_q \hat{i}_d \left(\frac{L_d}{L_q} - \frac{L_q}{L_d}\right)\right]$
If $g_{FSS} < g_{opt}$
$g_{opt} = g_{FSS}$
$\omega_{opt} = \omega_{FSS}$
End
If g_{opt} < accepted tolerance
Break
End
End
$\hat{\omega}_r = \omega_{opt}$
End

The block diagram for the overall system including the proposed sensor-less FSS-MRAS of the PMSG coupled to the wind turbine system is shown in Figure 5.

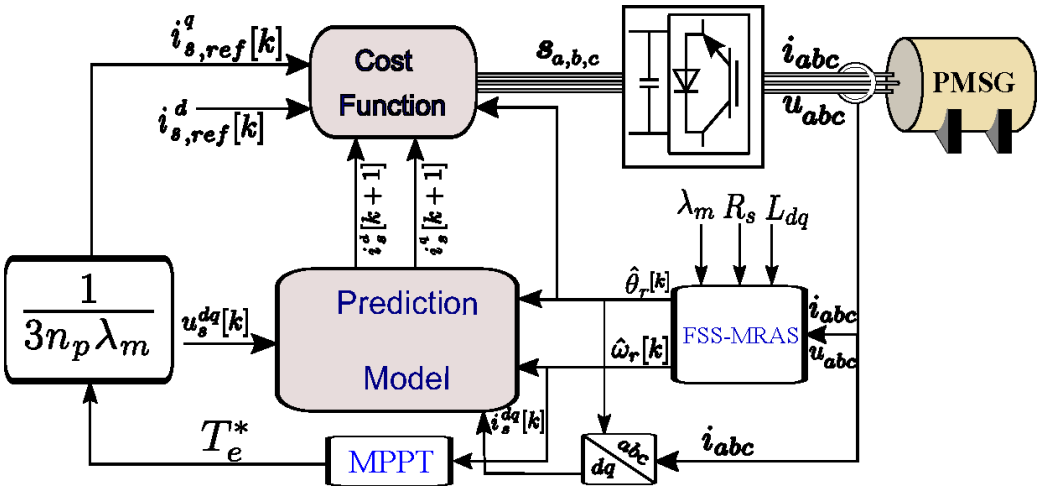

Figure 5. The proposed sensor-less FSS-MRAS estimator of the PMSG for a wind turbine system.

5. Simulation Results

To verify the suggested technique's robustness and capabilities, it is examined using Simulink and MATLAB M-File at various operating points. The wind turbine system and the PMSG have been built and the MPC algorithm is used to control the PMSG to obtain the MPPT of the wind turbine. Also, both the classical MRAS and the proposed FSS-MRAS techniques have been implemented in order to validate the proposed FSS-MRAS against the conventional MRAS. The rated parameters of the PMSG and wind turbine system are shown in Table 1.

Table 1. Parameters of the PMSG and wind turbine system.

Machine Parameters	Value
Wind turbine radius (m)	1.6
Rated wind speed (m/s)	15
Air density (kg/m^3)	1.22
Optimal tip speed ratio (λ^*)	8.11
Optimal power coefficient (C_p^*)	0.48
Pitch angle (β)	0
Magnetic pole pairs	4
Rated speed (rpm)	3000
Inertia J (kg·m^2)	0.011
Viscous damping coefficient B (N·m·s/rad)	0.001889
Stator resistance r_s (Ω)	0.05
flux linkage Ψ_f (wb)	0.192
Stator inductance (Ld = Lq) (H)	0.000635

In order to ensure the reliability and the capability of the speed estimation accuracy of the proposed FSS-MRAS, the proposed approach has been tested on variant operating points as follows.

5.1. Response of the Proposed FSS-MRAS at Rated Wind Speed

The FSS-MRAS has been tested at the rated high wind speed (15 m/s) to ensure the ability of the estimated speed to track the actual and conventional MRAS estimated speed. Figure 6 shows the response of the FSS-MRAS estimated speed against the actual and the conventional MRAS estimated speed. From Figure 6, it is obvious that the estimated speed of the proposed FSS-MRAS approach accurately tracks the reference speed and

the estimated speed of the conventional MRAS. Also, it is clear from the response that the average error between the speed of the proposed FSS-MRAS and the speed of the conventional MRAS converges to zero. Moreover, the estimated position of the proposed FSS-MRAS precisely tracks the estimated position of the conventional MRAS. As a result, the FSS-MRAS proved its capability in speed estimation at high wind speeds. In addition, the actual speed and the estimated speed of the FSS-MRAS and conventional MRAS achieve the speed reference, which also proves that the MPC can achieve the MPPT of the wind turbine system.

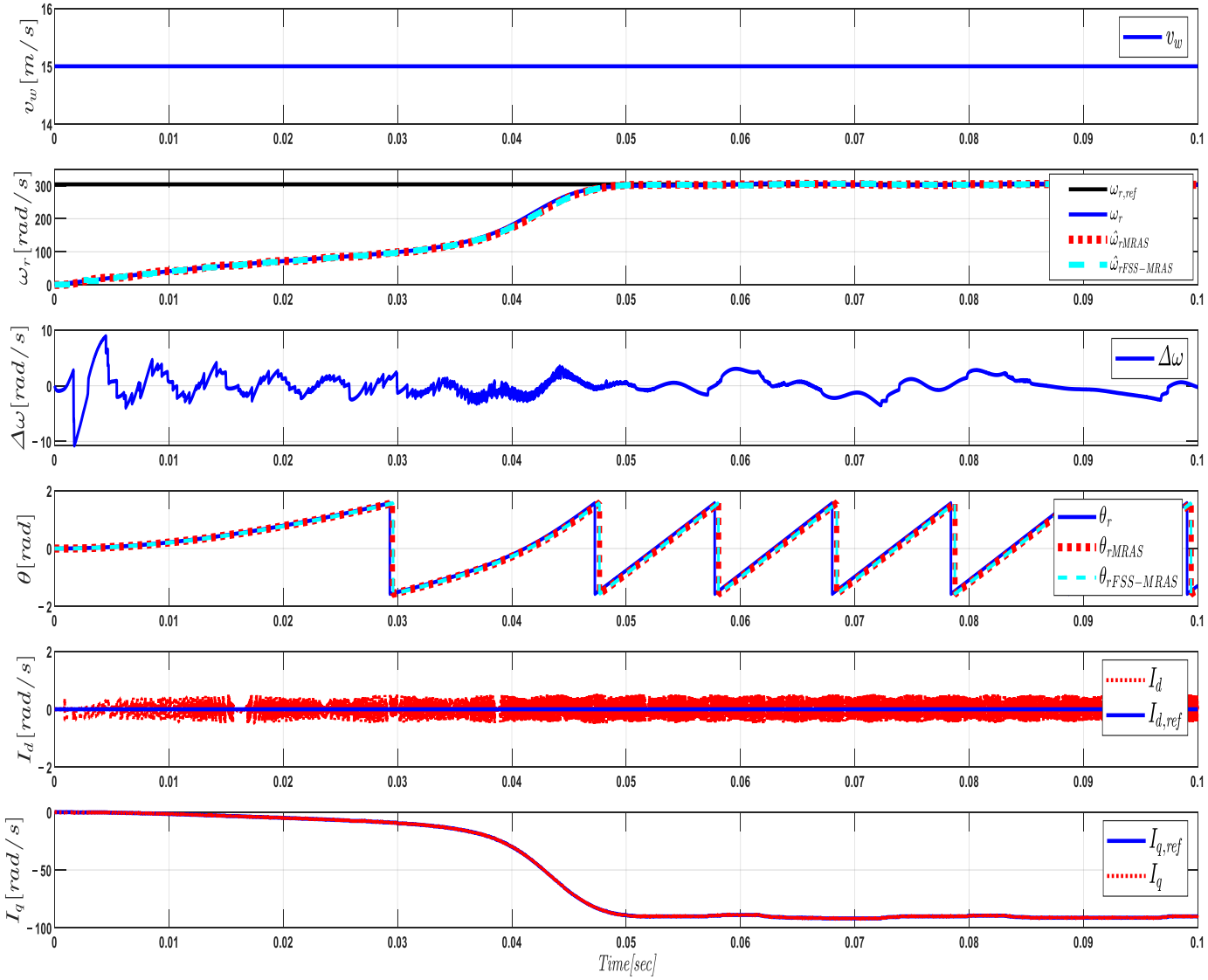

Figure 6. Simulation results of the proposed FSS-MRAS observer against the conventional MRAS at rated wind speed (15 m/s).

5.2. Response of the Proposed FSS-MRAS at Low Wind Speed

The presented FSS-MRAS algorithm has been validated at a low wind speed (5 m/s) to guarantee the reliability and robustness of the proposed FSS-MRAS's estimation performance and MPC control functionality. In Figure 7, the estimated speeds and positions of both the proposed FSS-MRAS and the conventional MRAS can achieve the reference speed with no overshoot, a good rise time, and no steady state error, which proves the perfect control performance of the MPC in harvesting the maximum power of the wind turbine. Furthermore, the superior speed/position estimation performance of the suggested FSS-MRAS to track the speed of the conventional MRAS is clearly shown in Figure 7 and the

error between the speeds of the conventional MRAS and the proposed FSS-MRAS is very small (almost zero on average).

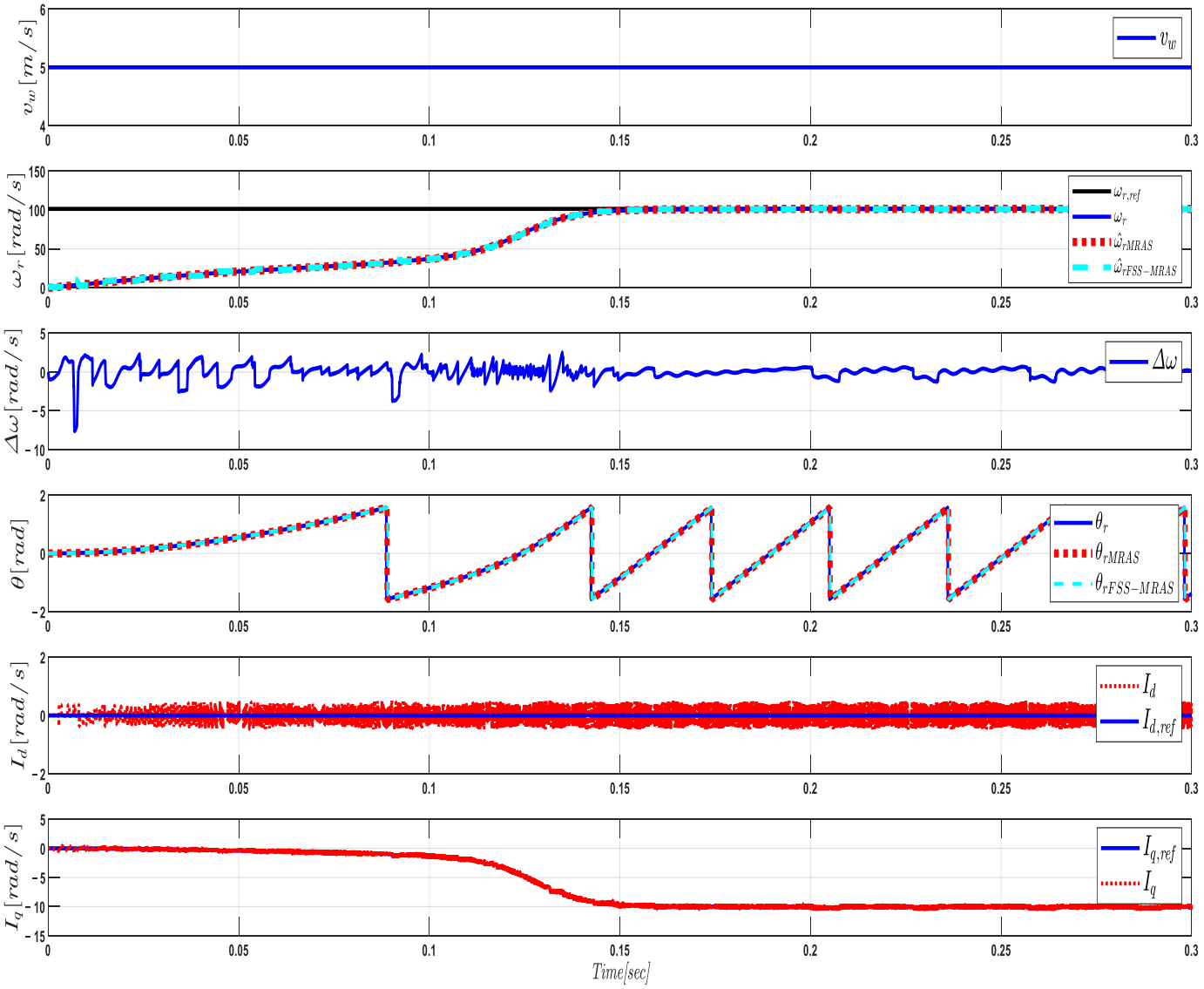

Figure 7. Simulation results of the proposed FSS-MRAS observer against the conventional MRAS at low wind speed (5 m/s).

5.3. Response of the Proposed FSS-MRAS at Variant Wind Speeds

Many variations of the wind speed are applied to verify the robustness of the proposed FSS-MRAS under variant dynamics. In Figure 8, the wind speed starts at 3.75 m/s, then jumps up to 7.5 m/s at 0.3 s, then rises to 11.25 m/s at 0.4 s, increases to 15 m/s at 0.5 s, then decreases by 3.75 m/s to reach 11.25 m/s at 0.6 s, then down to 7.5 m/s at 0.7 s and finally changes to 3.75 m/s at 0.8 s. Figure 8 evidently demonstrates that the estimated speed/position of the proposed FSS-MRAS technique correctly tracks the estimated speed/position of the conventional MRAS with very little error between them. Also, the measured speed, FSS-MRAS speed, and conventional MRAS speed attain the reference speed, which accomplishes the MPPT of the wind turbine. Consequently, both the MPC of the PMSG and the proposed estimation FSS-MRAS technique can apparently respond with a perfect performance at different variations in wind speed.

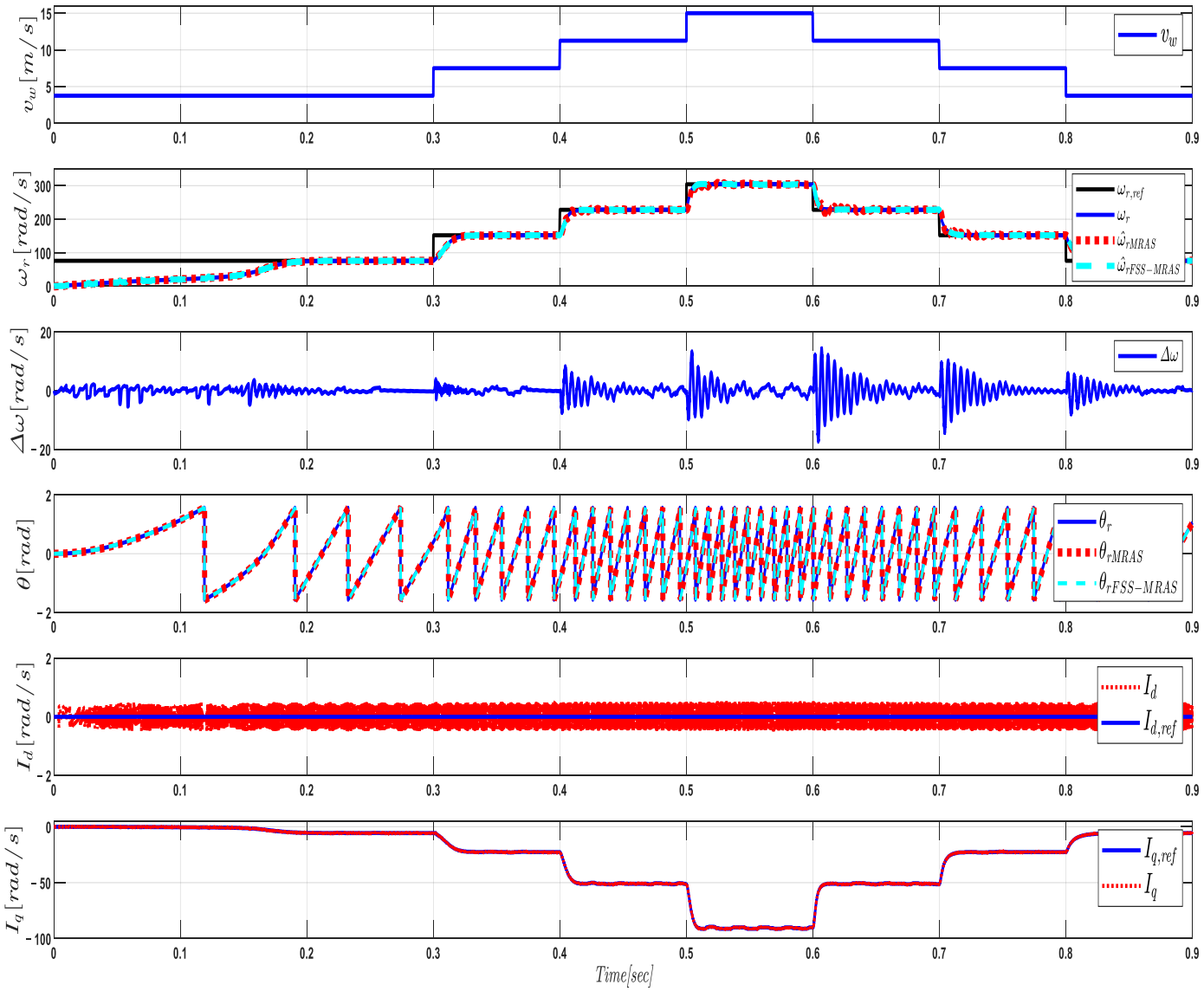

Figure 8. Performance of the proposed FSS-MRAS against the conventional observer at wide dynamics in wind speed.

5.4. Response of the Proposed FSS-MRAS at Variations of PMSG Resistance

The reliability of the proposed FSS-MRAS and the traditional MRAS are tested against variations of PMSG resistance. In Figure 9, the PMSG resistance decreases to 0.5 r_s (0.025 Ω) at 0.1 s then increases to 1.5 r_s (0.075 Ω) at 0.3 s. It is obvious from Figure 9 that the proposed FSS-MRAS technique proves its robustness and high capability at variations in PMSG resistance. Also, Figure 9 demonstrates that the FSS-MRAS presents low-speed oscillations at PMSG variations compared to the conventional one.

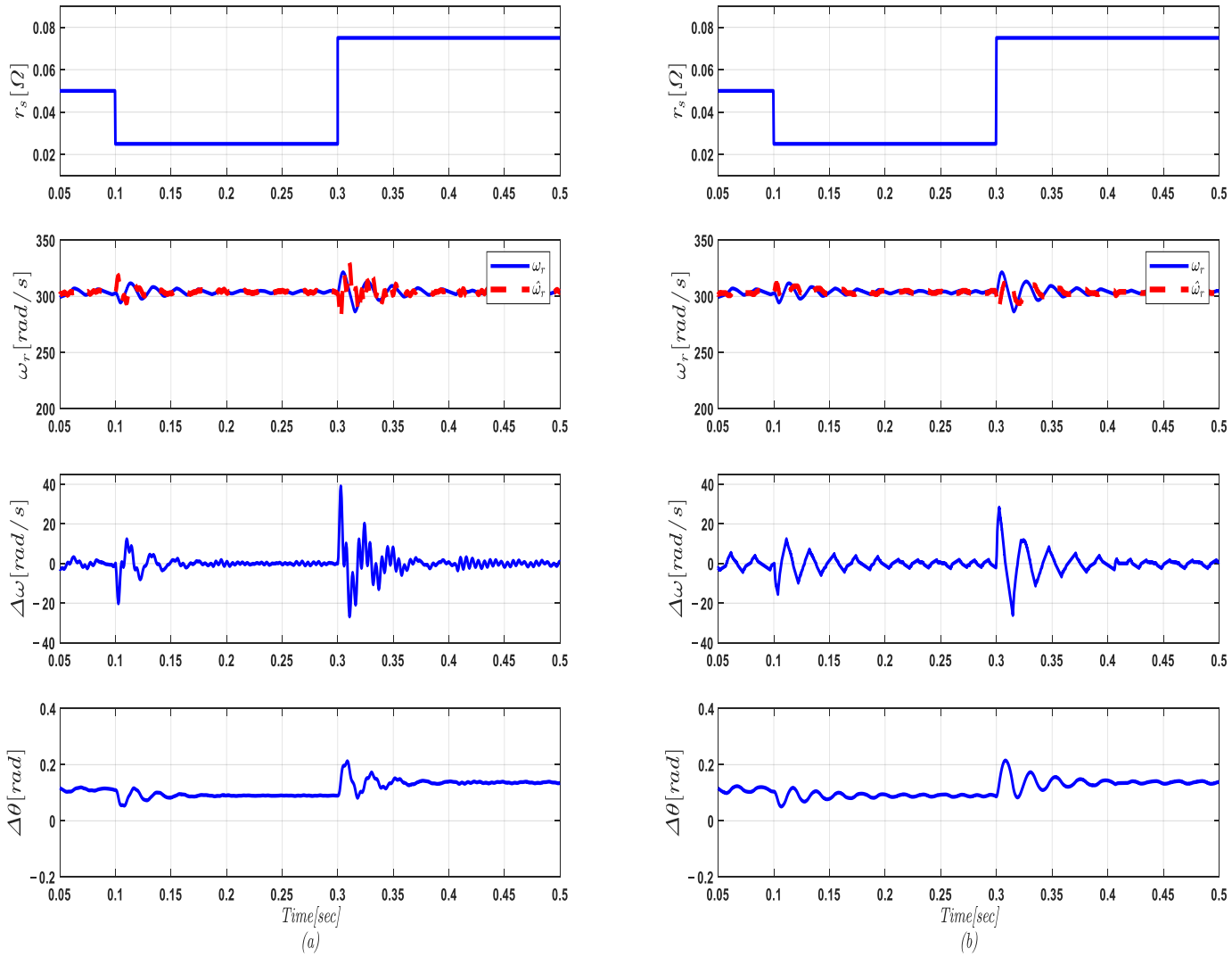

Figure 9. Performance of a proposed FSS-MRAS and a classical one at step variations of PMSG resistance: (**a**) traditional MRAS; (**b**) FSS-MRAS estimator.

5.5. Response of the Proposed FSS-MRAS at Variations of PMSG Inductance

The robustness of the presented FSS-MRAS and the classical one is examined at step changes of PMSG inductance. Figure 10 shows the step changes in PMSG inductances (L_d, L_q) for 0.75 of their values at 0.1 s and for 1.25 of their values at 0.3 s. Figure 10 proves the ability of the proposed FSS-MRAS to track the actual speed precisely. Also, Figure 10 shows lower ripples of the proposed FSS-MRAS compared to the conventional one at inductance changes.

From the previous results, it is clear that the proposed FSS-MRAS technique can achieve the same response as the conventional MRAS but without the employment of the PI controller, and consequently the tuning burden of the PI controller is omitted which leads to simplicity and adaptability of the proposed algorithm. Moreover, the proposed FSS-MRAS approach outperforms the classical MRAS at variations of PMSG resistance and inductance with lower ripples and oscillations in the speed response. Table 2 exhibits the variances between the two estimators in which the FSS-MRAS shows a better response compared to the conventional one, with lower ripples and overshoot at the PMSG's parameters changes.

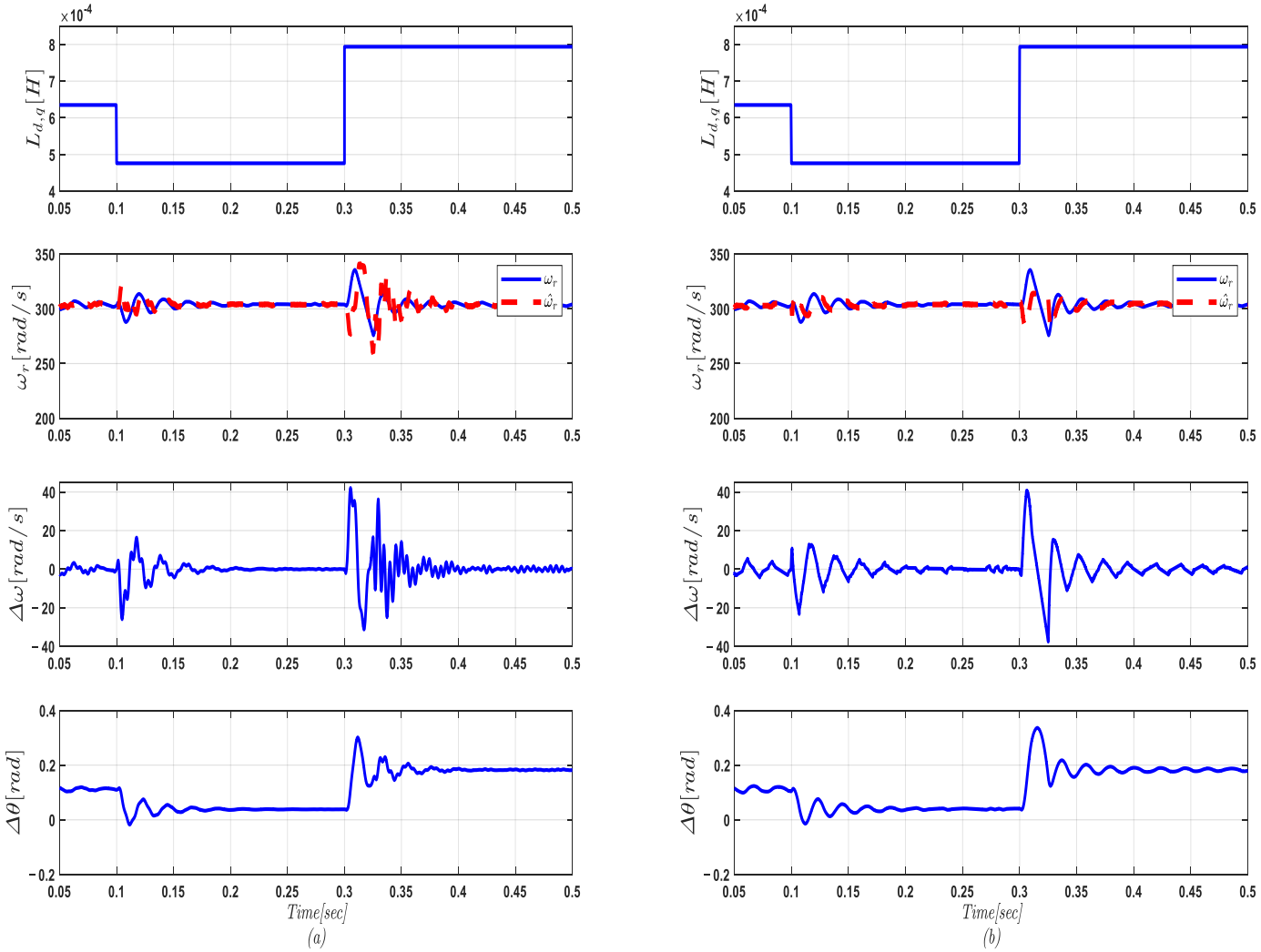

Figure 10. Performance of the proposed FSS-MRAS and the classical one at step variations of PMSG inductance: (**a**) traditional MRAS; (**b**) FSS-MRAS estimator.

Table 2. Functional comparison between the traditional MRAS and the proposed FSS-MRAS.

	Traditional MRAS	**FSS-MRAS**
Tracking Response	accurate	Accurate
Speed steady state error	zero	Zero
Response on R_s change	Accurate (low ripples) 10% overshoot	more accurate (lower ripples) (7% overshoot)
Response on L_s change	Accurate (low ripples) 11% overshoot	more accurate (lower ripples) (9% overshoot)

6. Conclusions

This paper proposed a finite speed-set model reference adaptive system (FSS-MRAS) to estimate the speed/position of the permanent magnet synchronous generator in the wind energy turbine system. The presented FSS-MRAS is based on the main concept of the FCS-MPC. The FSS-MRAS uses a limited set of speeds of the rotor that are employed to predict the rotor speed of the generator. Consequently, the optimal speed of the rotor is the one that its prediction optimizes from a predefined cost function. By the employment of the proposed FSS-MRAS, the classical MRAS PI controller is omitted and—as a result—the tuning difficulty is overcome. The proposed sensor-less FSS-MRAS has been tested and its

performance is compared with the classical MRAS. The simulation results displayed that the response of the investigated FSS-MRAS observer are slightly better than the conventional one, with low ripples and minimum steady state error. Furthermore, the proposed estimator illustrated sufficient robustness to the variation of generator parameters.

Author Contributions: M.M.A. and A.F. conceived, designed, and implemented the control strategies and wrote the manuscript; A.A.S. and M.A.H. were responsible for the guidance and a number of key suggestions. All authors have read and agreed to the published version of the manuscript.

Funding: This work was supported by the Deanship of Scientific Research, Vice Presidency for Graduate Studies and Scientific Research, King Faisal University, Saudi Arabia [GRANTA497].

Data Availability Statement: Data are contained within the article.

Conflicts of Interest: The authors declare no conflicts of interest.

Nomenclature

PMSG	Permanent magnet synchronous generator
CPC	Current predictive control
MPC	Model predictive control
DFIG	Doubly fed induction generator
WES	Wind energy system
FOC	Field oriented control
PMSG	Permanent magnet synchronous generator
CS-MPC	Continuous-set model predictive control
FS-MPC	Finite-set model predictive control
EKF	Extended Kalman filter
SMO	Sliding mode observer
PLL	Phase locked loop
MRAS	Model reference adaptive system
FSS-MRAS	Finite speed-set model reference adaptive system

References

1. Abdelrahem, M.; Hackl, C.; Kennel, R. Model Predictive Control of Permanent Magnet Synchronous Generators in Variable-Speed Wind Turbine Systems. In Proceedings of the Power and Energy Student Summit (PESS 2016), Aachen, Germany, 19–20 January 2016; pp. 19–20. Available online: https://api.semanticscholar.org/CorpusID:58979165 (accessed on 1 May 2024).
2. Datta, R.; Ranganathan, V.T. Variable-Speed Wind Power Generation Using Doubly Fed Wound Rotor Induction Machine-a Comparison with Alternative Schemes. *IEEE Trans. Energy Convers.* **2002**, *17*, 414–421. [CrossRef]
3. Li, H.; Chen, Z. Overview of Different Wind Generator Systems and Their Comparisons. *IET Renew. Power Gener.* **2008**, *2*, 123–138. [CrossRef]
4. Phan, T.T.; Nguyen, V.L.; Hossain, M.J.; To, A.N.; Tran, H.T.; Phan, T.N. Transient Responses of the Doubly-Fed Induction Generator Wind Turbine under Grid Fault Conditions. In Proceedings of the 2016 International Conference on Advanced Computing and Applications (ACOMP), Can Tho City, Vietnam, 23–25 November 2016; pp. 97–104.
5. Zarei, M.E.; Ramirez, D.; Prodanovic, M.; Arana, G.M. Model Predictive Control for PMSG-Based Wind Turbines with Overmodulation and Adjustable Dynamic Response Time. *IEEE Trans. Ind. Electron.* **2021**, *69*, 1573–1585. [CrossRef]
6. Nasir Uddin, M.; Patel, N. Maximum Power Point Tracking Control of IPMSG Incorporating Loss Minimization and Speed Sensorless Schemes for Wind Energy System. *IEEE Trans. Ind. Appl.* **2016**, *52*, 1902–1912. [CrossRef]
7. Saleh, S.A.M. Testing the Performance of a Resolution-Level MPPT Controller for PMG-Based Wind Energy Conversion Systems. *IEEE Trans. Ind. Appl.* **2017**, *53*, 2526–2540. [CrossRef]
8. Calabrese, D.; Tricarico, G.; Brescia, E.; Cascella, G.L.; Monopoli, V.G.; Cupertino, F. Variable Structure Control of a Small Ducted Wind Turbine in the Whole Wind Speed Range Using a Luenberger Observer. *Energies* **2020**, *13*, 4647. [CrossRef]
9. Nasiri, M.R.; Farhangi, S.; Rodriguez, J. Model Predictive Control of a Multilevel CHB STATCOM in Wind Farm Application Using Diophantine Equations. *IEEE Trans. Ind. Electron.* **2018**, *66*, 1213–1223. [CrossRef]
10. Karamanakos, P.; Geyer, T. Guidelines for the Design of Finite Control Set Model Predictive Controllers. *IEEE Trans. Power Electron.* **2019**, *35*, 7434–7450. [CrossRef]

11. Ding, H.; Zou, X.; Li, J. Sensorless Control Strategy of Permanent Magnet Synchronous Motor Based on Fuzzy Sliding Mode Observer. *IEEE Access* **2022**, *10*, 36743–36752. [CrossRef]
12. Liu, Z.-H.; Nie, J.; Wei, H.-L.; Chen, L.; Li, X.-H.; Lv, M.-Y. Switched PI Control Based MRAS for Sensorless Control of PMSM Drives Using Fuzzy-Logic-Controller. *IEEE Open J. Power Electron.* **2022**, *3*, 368–381. [CrossRef]
13. Ahmed, W.A.E.M.; Adel, M.M.; Taha, M.; Saleh, A.A. PSO Technique Applied to Sensorless Field-Oriented Control PMSM Drive with Discretized RL-Fractional Integral. *Alexandria Eng. J.* **2021**, *60*, 4029–4040. [CrossRef]
14. Liyong, Y.; Peie, Y.; Zhenguo, C.; Zhigang, C.; Zhengxi, L. A Novel Control Strategy of Power Converter Used to Direct Driven Permanent Magnet Wind Power Generation System. In Proceedings of the 2009 2nd International Conference on Power Electronics and Intelligent Transportation System (PEITS), Shenzhen, China, 19–20 December 2009; Volume 1, pp. 456–459.
15. Yang, L.; Chen, Z.; Yuan, P.; Chang, Z. A Novel Fuzzy Logic and Anti-Windup PI Controller for a Rectifier with Direct Driven Permanent Magnet Synchronous Generator. In Proceedings of the 2009 2nd International Conference on Power Electronics and Intelligent Transportation System (PEITS), Shenzhen, China, 19–20 December 2009; Volume 2, pp. 422–426.
16. Shariatpanah, H.; Fadaeinedjad, R.; Rashidinejad, M. A New Model for PMSG-Based Wind Turbine with Yaw Control. *IEEE Trans. Energy Convers.* **2013**, *28*, 929–937. [CrossRef]
17. Corradini, M.L.; Ippoliti, G.; Orlando, G. Robust Control of Variable-Speed Wind Turbines Based on an Aerodynamic Torque Observer. *IEEE Trans. Control Syst. Technol.* **2013**, *21*, 1199–1206. [CrossRef]
18. Benadja, M.; Chandra, A. Adaptive Sensorless Control of PMSGs-Based Offshore Wind Farm and VSC-HVdc Stations. *IEEE J. Emerg. Sel. Top. Power Electron.* **2015**, *3*, 918–931. [CrossRef]
19. Abdelrahem, M.; Hackl, C.M.; Kennel, R. Finite Position Set-Phase Locked Loop for Sensorless Control of Direct-Driven Permanent-Magnet Synchronous Generators. *IEEE Trans. Power Electron.* **2017**, *33*, 3097–3105. [CrossRef]
20. Abdelrahem, M.; Hackl, C.M.; Kennel, R.; Rodriguez, J. Computationally Efficient Finite-Position-Set-Phase-Locked Loop for Sensorless Control of PMSGs in Wind Turbine Applications. *IEEE Trans. Power Electron.* **2020**, *36*, 3007–3016. [CrossRef]
21. Abdelrahem, M.; Hackl, C.; Farhan, A.; Kennel, R. Finite-Set MRAS Observer for Encoderless Control of PMSGs in Wind Turbine Applications. In Proceedings of the 2019 IEEE Conference on Power Electronics and Renewable Energy (CPERE), Aswan City, Egypt, 23–25 October 2019; pp. 431–436.
22. Abdelrahem, M.; Hackl, C.M.; Rodríguez, J.; Kennel, R. Model Reference Adaptive System with Finite-Set for Encoderless Control of PMSGs in Micro-Grid Systems. *Energies* **2020**, *13*, 4844. [CrossRef]
23. Abdelrahem, M.; Hackl, C.M.; Kennel, R. Limited-Position Set Model-Reference Adaptive Observer for Control of DFIGs without Mechanical Sensors. *Machines* **2020**, *8*, 72. [CrossRef]
24. Elbeji, O.; Hannachi, M.; Benhamed, M.; Sbita, L. Artificial Neural Network—Based Sensorless Control of Wind Energy Conversion System Driving a Permanent Magnet Synchronous Generator. *Wind Eng.* **2021**, *45*, 459–476. [CrossRef]
25. Wu, B.; Lang, Y.; Zargari, N.; Kouro, S. *Power Conversion and Control of Wind Energy Systems*; John Wiley & Sons: Hoboken, NJ, USA, 2011; Volume 76.
26. Abdelrahem, M.; Hackl, C.; Kennel, R. Robust Predictive Control Scheme for Permanent-Magnet Synchronous Generators Based Modern Wind Turbines. *Electronics* **2021**, *10*, 1596. [CrossRef]
27. Sun, Y.; Zhao, Y.; Dou, Z.; Li, Y.; Guo, L. Model Predictive Virtual Synchronous Control of Permanent Magnet Synchronous Generator-Based Wind Power System. *Energies* **2020**, *13*, 5022. [CrossRef]
28. Abdelrahem, M.; Hackl, C.; Kennel, R.; Rodriguez, J. Sensorless Predictive Speed Control of Permanent-Magnet Synchronous Generators in Wind Turbine Applications. In Proceedings of the PCIM Europe 2019; International Exhibition and Conference for Power Electronics, Intelligent Motion, Renewable Energy and Energy Management, Nuremberg, Germany, 7–9 May 2019; pp. 1–8.
29. Farhan, A.; Abdelrahem, M.; Saleh, A.; Shaltout, A.; Kennel, R. Simplified Sensorless Current Predictive Control of Synchronous Reluctance Motor Using Online Parameter Estimation. *Energies* **2020**, *13*, 492. [CrossRef]
30. Farhan, A.; Abdelrahem, M.; Hackl, C.M.; Kennel, R.; Shaltout, A.; Saleh, A. Advanced Strategy of Speed Predictive Control for Nonlinear Synchronous Reluctance Motors. *Machines* **2020**, *8*, 44. [CrossRef]
31. Farhan, A.; Abdelrahem, M.; Saleh, A.; Shaltout, A.; Kennel, R. Robust Sensorless Direct Speed Predictive Control of Synchronous Reluctance Motor. In Proceedings of the 2020 IEEE 29th International Symposium on Industrial Electronics (ISIE), Delft, The Netherlands, 17–19 June 2020; pp. 1541–1546.
32. Farhan, A.; Abdelrahem, M.; Shaltout, A.; Kennel, R.; Saleh, A. Encoderless Current Predictive Control of Synchronous Reluctance Motor by Extended Kalman Filter Based State Estimation. In Proceedings of the PCIM Europe Digital Days 2020; International Exhibition and Conference for Power Electronics, Intelligent Motion, Renewable Energy and Energy Management, Nuremburg, Germany, 7–8 July 2020; pp. 1–8.
33. Farhan, A.; Saleh, A.; Abdelrahem, M.; Kennel, R.; Shaltout, A. High-Precision Sensorless Predictive Control of Salient-Pole Permanent Magnet Synchronous Motor Based-on Extended Kalman Filter. In Proceedings of the 2019 21st International Middle East Power Systems Conference (MEPCON), Cairo, Egypt, 17–19 December 2019; pp. 226–231.

34. Demir, R. Speed-Sensorless Predictive Current Controlled PMSM Drive with Adaptive Filtering-Based MRAS Speed Estimators. *Int. J. Control Autom. Syst.* **2023**, *21*, 2577–2586. [CrossRef]
35. Adel, M.M.; Saleh, A.A.; Hassan, M.A.; Kennel, R.; Farhan, A. Efficient Sensorless Speed Predictive Control Without Weighting Factors for PMSM Drive Based on MRAS Estimator. *J. Appl. Sci. Eng.* **2024**, *27*, 3697–3710. [CrossRef]